Simulations of turbulent flow between a rotating and a stationary disk

Magne Lygren

Department of Applied Mechanics,
Thermodynamics and Fluid Dynamics
Norwegian University of Science and Technology

February 2001

Summary

The main focus of this thesis is turbulent flow between a rotating and a stationary disk. The extension of the disks is assumed to be large enough to prevent the outer boundary conditions to influence the flow at the region of interest. This flow is driven by the shear between the disks, but an imbalance between centrifugal and pressure forces in the radial direction induces a radial cross-flow. The result is a complex three-dimensional flow where the direction of the mean flow varies with the axial position. Direct numerical simulations (DNS) and large eddy simulations (LES) have been used to investigate the flow. The simulations utilized a special set of quasi-periodic boundary conditions which allowed the use of a computational domain which captured only a section of the flow.

Locally, the disk flow is characterized by a rotational Reynolds number and a local gap ratio. A DNS was performed at a rotational Reynolds number of $4 \cdot 10^5$ and a gap ratio of 0.02. Turbulence statistics were compared to results from the turbulent plane Couette flow and from an experimental investigation of an enclosed rotor-stator flow. The plane Couette flow is a two-dimensional equivalence to the flow between the disks. Although the turbulence statistics had many similarities in the two cases, there were differences caused by three-dimensionality of the mean-flow in the disk case. In the disk flow the direction of the Reynolds shear stress vector was not aligned with the mean-gradient vector, and the ratio of the magnitude of the shear stress vector to the mean turbulent kinetic energy was reduced compared to the Couette flow.

The flow between the disks is statistically stationary. It is therefore a suitable case for studying effects of mean-flow three-dimensionality on the underlying coherent structures in the boundary layers. Ensemble averages, probability-density functions and a quadrant analysis of conditional averages in the regions near the disks were performed in order to study the coherent quasi-streamwise vortices. By comparing with corresponding conditional averages from the near-wall region in the Poiseuille flow, the most dominant effect of the three-dimensionality on the vortices was found to be a reduction of the strength of sweeps that the vortices generate. The three-dimensionality also led to an asymmetry between vortices of different sign of rotation.

LES was used to study the flow at higher rotational Reynolds numbers and larger gap ratios. A mixed dynamic subgrid-scale model was used in the simulations. For a given gap between the disks, the degree of three-dimensionality of the mean-flow was reduced by increasing the Reynolds number. And as the Reynolds number increased, both second order turbulence statistics and conditional averages showed an increasing similarity with data in two-dimensional

boundary layers.

The final part of the thesis deals with the turbulent plane Couette flow. The development of a multigrid Poisson solver allowed non-conventional periodic boundary conditions to be specified in the streamwise direction of the flow. The motivation was to investigate the influence of boundary conditions on the formation of large-scale quasi-stable roll-cells observed only in numerically generated Couette flow. The non-conventional boundary conditions did influence these roll-cell, but the computational domain used was not large enough to allow firm conclusions to be drawn regarding the existence of the roll cells.

Preface

I would like to express my appreciations to my supervisor, Professor Helge I. Andersson, for his guidance and inspiration throughout the work on this thesis.

Thanks are also due to Associate Professor Reidar Kristoffersen for introducing me to computer codes and for solving all kinds of computer issues. I would also like to thank my fellow dr. ing. students for making an enjoyable and inspiring environment at the Division of Applied Mechanics. Especially I would like to thank Peter S. Johansson and Tarek Yousef for revising the introduction of this thesis and one of the papers.

Professor Kyle D. Squires at Arizona State University has been very helpful in discussions on numerical issues.

This research was funded by The Research Council of Norway under contract no. 115548/410. This work has also received support from The Research Council of Norway (Programme for Supercomputing) through a grant of computing time on the CRAY J90 in Trondheim.

Special thanks go to my wife Brit. Particularly during the latest months of this work she has taken the far greatest responsibility for taking care of our children and for keeping the family going. Her encouragement and support is highly appreciated.

Bryne, February 2001

Magne Lygren

Contents

Introduction

This thesis consists of an introduction and seven appended papers. The papers are self-contained with abstracts and references. The flow between a rotating and a stationary disk is studied in five of the papers. Simulations of the plane Couette flow are presented in the remaining two papers.

1 Motivation and objectives

The interest in rotor-stator flows is twofold. Firstly, these flows are found in turbomachinery, and detailed knowledge of the flow conditions is needed in improvement of their performance. Secondly, these flows are of fundamental interest.

In real rotor-stator configurations the geometry may be very complex. Depending on the rotational speed, boundary layers are formed near solid boundaries. Due to an imbalance between pressure- and centrifugal forces the flow near the rotor is directed outwards while near the stator it is directed towards the axis of rotation.

Most practical rotor-stator flows are turbulent. The turbulent flow in these systems needs to be examined more carefully in order to be better understood. The boundary layers near the rotor and the stator are examples of so-called three-dimensional boundary layers, i.e. the direction of the mean flow is not constant throughout the boundary layers. This three-dimensionality may affect the turbulence in the boundary layers resulting in e.g. lower drag than in ordinary two-dimensional boundary layers. Most turbulence models are validated against two-dimensional flows and the performance of the models is often poor when applied to three-dimensional boundary layers.

The objective of this thesis is to study the turbulent flow in a simplified rotor-stator system. The configuration considered consists of two parallel "infinite" disks where one is rotating with constant angular velocity and the other is stationary. The flow is studied by direct numerical simulations and large eddy simulations. Turbulence statistics useful for validations of turbulence models are generated for different gap ratios and Reynolds numbers. Coherent structures in the boundary layers are analyzed in detail in order to increase the understanding of the generation of turbulence, both in rotor-stator flows as well as in three-dimensional turbulent boundary layers in general.

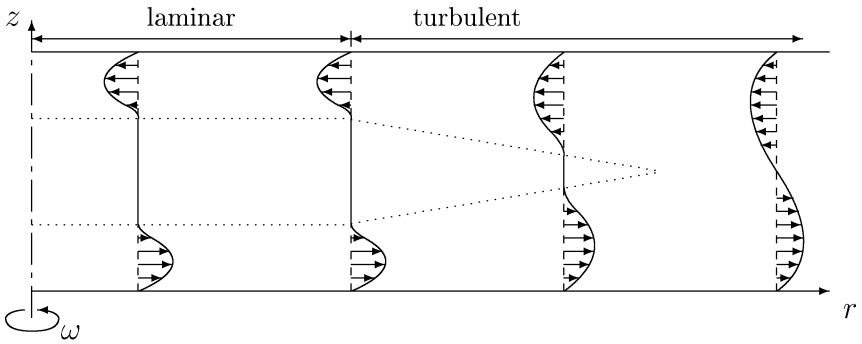

Figure 1: Profiles of the radial velocity component in the gap between a rotating and a stationary disk. The profiles illustrate the development from separated to merged boundary layers with increasing r.

2 Rotor-stator flows

The flow in simplified rotor-stator configurations can be divided into four different flow regimes. This was first recognized by Daily & Nece (1960) who performed experimental work on enclosed disks with different gap widths and rotation rates. They identified the following flow-regimes: Regime I characterized by merged laminar boundary layers, regime II having separated laminar boundary layers (separated by a region of fluid with constant angular velocity), regime III with merged turbulent boundary layers and regime IV with separated turbulent boundary layers. The enclosed flow is characterized by the rotational Reynolds number $Re_R = R^2\omega/\nu$ and the gap ratio $G_R = s/R$, where R is the radius of the disks, ω the angular frequency of the rotating disk, ν the kinematic viscosity while s the axial distance between the disks.

Near the axis of rotation, Daily & Nece (1960) found that the flow was laminar. If Re_R was large enough, the flow would undergo transition to turbulence further out from the axis of rotation. The situation is illustrated in figure 1 where the boundary layer structure in the large gap between two disks is shown. For sufficiently small gaps the boundary layers are merged in the laminar region as well.

2.1 Laminar flow

For laminar flow over one rotating disk von Karman (1921) assumed that the velocity (u_r, u_θ, u_z) of the fluid was such that $u_r/r\omega$, $u_\theta/r\omega$ and u_z were independent of r. The Navier-Stokes equation could thereby be reduced to a set of ordinary differential equations (ODEs) depending only on the axial coordinate. Bodewadt (1940) extended this analysis to allow the outer flow be in solid-body rotation. Batchelor (1951) included a parallel coaxial disk and used the von Karman similarity assumptions to develop a set of ODEs.

Following the von Karman similarity principle, the velocity components are expressed as

$$u_r = r\omega f'(x), \qquad u_\theta = r\omega g(x), \qquad u_z = -2(\nu\omega)^{1/2} f(x). \tag{1}$$

Here the prime means differentiation with respect to the non-dimensional axial coordinate $x = z(\omega/\nu)^{1/2}$. The stationary Navier-Stokes equations now reduce to the similarity equations

$$f'''' + 2ff'' = -2gg', \tag{2}$$

$$g'' + 2fg' = 2f'g, \tag{3}$$

with boundary conditions (only one disk rotating at $x = 0$)

$$f(0) = f'(0) = f(Re_s^{1/2}) = f'(Re_s^{1/2}) = g(Re_s^{1/2}) = 0, \tag{4}$$

$$g(0) = 1, \tag{5}$$

where $Re_s = s^2\omega/\nu$ is the gap Reynolds number. Note that the stationary disk is located at $x = Re_s^{1/2}$. Batchelor (1951) argued that for large Re_s boundary layers form near both disks and the fluid in the core rotates with a constant angular velocity. Stewartson (1953), on the other hand, obtained low-Reynolds number power-series solutions to the similarity equations and concluded that for higher Reynolds numbers a boundary layer would exist only near the rotating disk. In the core-region the fluid would not rotate.

These conflicting conclusions have triggered several investigations on rotating disk flow. The early numerical solutions by Lance & Rogers (1962) and Pearson (1965) indicated that the Batchelor type of solution was correct. Later Mellor *et al.* (1968) showed that both the Batchelor type and the Stewartson type of solution exist at high Reynolds numbers. Important works on this flow by Nguyen *et al.* (1975); Roberts & Shipman (1976); Holodniok *et al.* (1977, 1981); Szeto (1978) and Keller & Szeto (1980) revealed the complex structure of similarity equations. Szeto (1978), e.g., showed that the solution is unique when Re_s is below 55 and that a myriad of different solutions emerge when Re_s increases. The temporal stability was also analyzed by Szeto (1978) revealing that the Batchelor solution is stable while the Stewartson solution is unstable. Work on the flow over one disk as well as the flow between two disks is reviewed in an article by Zandbergen & Dijkstra (1987).

Holodniok *et al.* (1977, 1981) used finite-differences and Newton iterations to solve the similarity equations. For higher Re_s this method was found to be unstable, and Holodniok *et al.* (1981) concluded that multiple shooting techniques would give more stable solutions. To get an impression of the Batchelor solutions to the similarity equations (2) and (3), the equations are here solved for a range of Re_s. Figure 2 shows the tangential and radial velocity components. For Re_s smaller than 1000, a single shooting technique is used, based on a fourth order Runge-Kutta solver in the numerical computer program MATLAB. When Re_s is 1000 or larger, multiple shooting is necessary to make the solution stable.

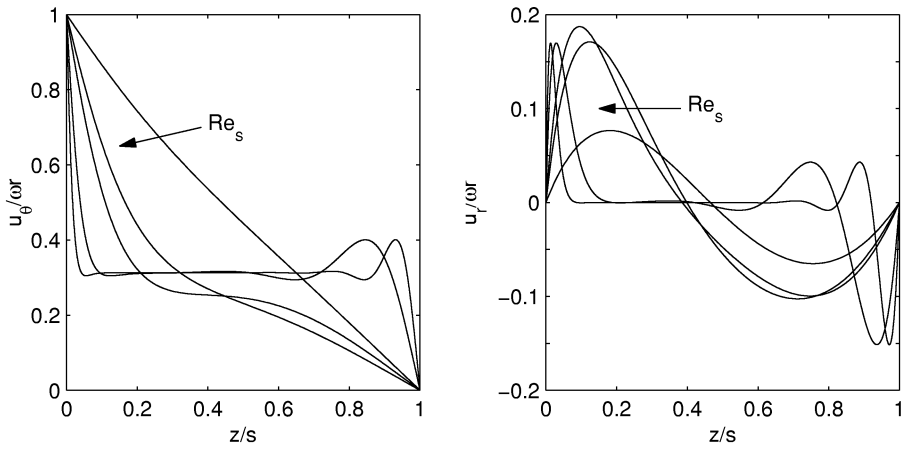

Figure 2: Solutions to the von Karman similarity equations for Reynolds numbers $Re_s = 10, 50, 100, 1000$ and 5000. As Re_s increases the thickness of the boundary layers decreases.

For low Re_s the tangential velocity profile approaches the streamwise profile of the plane Couette flow. When the Reynolds number increases, the thickness of the boundary layer decreases, and the tangential velocity is constant in the core. The limiting value of u_θ is approximately 0.313 in the core for high Re_s.

2.2 Stability and transition

For a given disk-separation, the flow will undergo transition to turbulence at a critical local Reynolds number $Re_r = r^2\omega/\nu$. This is indicated in figure 1. Experiments on confined rotor-stator flows have shown that circular and spiral waves are involved in the instability process, see e.g. the recent papers by Schouveiler (1998); Gauthier *et al.* (1999) and Schouveiler *et al.* (1999) and references therein. The first instabilities were axisymmetric circular waves moving inwards near the stationary disk occurring at a (global) Reynolds number Re_R of order 10^3, depending on the gap width. With increasing Reynolds number spiral wave patterns were formed.

In experiments by Itoh *et al.* (1992), Itoh (1995) and Cheah *et al.* (1994), the flow was turbulent except in a region near the axis of rotation. Near the stationary disk the flow was turbulent at almost all radial positions, while near the rotating disk the transition to turbulence took place typically between $Re_r = 1.6 \cdot 10^6$ and $Re_r = 3.6 \cdot 10^6$. From these experiments it is also seen that the radial position of the transition depends on both the local rotational Reynolds number and the local gap ratio.

2.3 Turbulent flow

Relatively few experimental investigations of turbulent rotor-stator flow have been reported in the literature. The first reported experiment on turbulent rotor-stator flow was by Daily & Nece (1960). They measured the tangential and radial mean velocities, mean pressure distribution as well as the frictional torque on the rotating disk. The Reynolds number Re_R varied between 10^3 and 10^7 and the gap ratio G_R was 0.0127, 0.0355, 0.0637, 0.115 and 0.217. Later Itoh *et al.* (1992); Itoh (1995) and Cheah *et al.* (1994) reported measurements on mean velocities as well as second order statistics in enclosed geometries with the outer shroud being stationary. Kilic *et al.* (1996) measured mean velocities of the flow at $Re_R = 1.25 \cdot 10^6$ and $G_R = 0.12$.

Theoretically, the flow between a rotating and a stationary disk has been treated by Owen & Rogers (1989). By assuming that there is an inviscid rotating core rotating with a constant angular velocity $\beta\omega$, the two boundary layers could be treated separately. In their analysis they used 1/7-power-profiles for the velocity in the boundary layers, giving $\beta = 0.431$. In the experiment by Daily & Nece (1960), β varied from 0.412 to 0.460 for different gap ratios. Itoh *et al.* (1992) found that β was between 0.40 and 0.42.

A larger number of numerical studies of this flow using turbulence modeling have been performed. Cooper & Reshotko (1975) used an effective-viscosity turbulence model and a switching factor to enforce a fully turbulent flow at $Re_r = 3 \cdot 10^5$. Morse (1991) forced the transition to occur by increasing the turbulence energy production term in his modified version of the low Reynolds number $k-\epsilon$ turbulence model by Launder & Sharma (1974). The mean velocity components in these two calculations were in reasonable good agreement with experiments. More recently Elena & Schiestel (1995) treated the flow with three different models, namely a low Reynolds number $k-\epsilon$ model, an algebraic stress model linked to the $k-\epsilon$ model near the wall, and a full Reynolds stress transport closure. Comparing with the experiments by Itoh *et al.* (1992), the level of the angular frequency in the core region was not correctly estimated by neither of the models, and the predicted flow near the rotating disk was almost laminar. Near the stationary disk the algebraic stress model and the Reynolds stress model predicted a turbulent flow, but the level of the turbulence was poorly predicted. Using a refined Reynolds stress model, Randriamampianina *et al.* (1997) predicted a turbulent flow near the rotor, in accordance with experiments. However, the level of the turbulence was low near the rotor.

There are several reasons for the difficulties in the performance of the turbulence models. Since the transition from laminar to turbulent flow first takes place in the boundary layer near the stationary disk, laminar and turbulent flow coexist for a radial region. The radial position of the transition point also has to be predicted. The effect of rotation of the flow influences the turbulence directly through centrifugal and Coriolis effects. But the effect is also more subtle like the influence from the induced mean-flow three-dimensionality on the turbulence. One aim of performing simulations of the flow between a rotating and a stationary disk is to shed light on some of these effects.

3 Three-dimensional turbulent boundary layers

A boundary layer is three-dimensional when the direction of the mean flow varies with the distance from the wall. There are basically two kinds of three-dimensional turbulent boundary layers (3DTBLs). Firstly, there are "non-stationary" or "spatially evolving" 3DTBLs. Secondly, there are "stationary" 3DTBLs. In flows of the first kind, mean velocities and turbulence statistics vary rapidly with time or with spatial position. Typically an initially two-dimensional flow experiences a sudden (either in time or in space) perturbation leading to a three-dimensional flow. An example is the flow meeting the spanwise pressure gradient from a swept wing. These flows are studied by e.g. Bradshaw & Pontikos (1985); Moin *et al.* (1990); Le *et al.* (1999) and Coleman *et al.* (2000). Flows of the second kind are stationary in time, but may vary slowly with the spatial position. These flows are typically subjected to continuous body-forces acting in the spanwise direction, such as centrifugal or Coriolis forces. Examples are the turbulent Ekman layer and the flow over a rotating disk. Stationary 3DTBLs have previously been studied by e.g. Spalart (1989); Coleman *et al.* (1990); Littell & Eaton (1994) and Wu & Squires (2000).

The turbulent flow between a rotating and a stationary disk belongs to stationary 3DTBLs. In this thesis the study of effects of the three-dimensionality on the underlying turbulence structures is an important issue. In non-stationary boundary layers other effects than the three-dimensionality may strongly influence the turbulence. In the flow over a swept wing, e.g., the adverse pressure gradient may modify the turbulence more strongly than the three-dimensionality (Coleman *et al.*, 2000). By studying stationary 3DTBLs, differences in turbulence structures as compared to those found in 2DTBLs are therefore more likely to be associated by the three-dimensionality alone. In the introduction of paper I an overview of the turbulence structures observed in 2D and 3D turbulent boundary layers are given.

4 Numerical simulations

The flows considered in this thesis are studied by means of direct numerical simulation (DNS) and large eddy simulation (LES). In a DNS the Navier-Stokes equations are solved numerically in space and time capturing all essential time- and length-scales. In a LES the large energy-containing eddies are computed, while the small scales are subjected to modeling.

The first DNSs were of isotropic turbulence in the early seventies (Orszag & Patterson, 1972). Simulations of wall-bounded turbulence were first reported by Moser & Moin (1987) who considered a curved channel flow, and by Kim *et al.* (1987) who studied the plane channel. Later the turbulent flat plate boundary layer was computed by Spalart (1988). Keeping the geometry simple, the simulated flows have increased in physical complexity to include e.g. three-dimensionality (Moin *et al.*, 1990), rotation (Kristoffersen & Andersson, 1993), body-forces (Coleman *et al.*, 1990), compressibility (Coleman *et al.*, 1995) and

interaction of turbulence with shock waves (Lee *et al.*, 1997). The flow over a backward facing step (Le *et al.*, 1997) and flat plate boundary layer separation (Na & Moin, 1998) are examples of simulated flows with an increasing geometric complexity. For a recent review article on DNS, see Moin & Mahesh (1998).

In LES of turbulence, the smallest scales are not explicitly solved and have to be modeled. Large and small scales are separated by spatially filtering of the flow variables. By applying the filter to the incompressible Navier-Stokes equations, the so-called subgrid-scale (SGS) stresses $\tau_{ij} = \overline{u_i u_j} - \overline{u}_i \overline{u}_j$ are introduced. Here, an overbar denotes filtering of the variables. These quantities are not resolved by the computational grid (thereby the name subgrid-scale), and a SGS model has to be applied in order to close the filtered Navier-Stokes equations. Most of the LES closures are based on the Smagorinsky model (Smagorinsky, 1963) which relates the deviatoric part of the SGS stress tensor τ_{ij} to the resolved strain-rate tensor $\overline{S}_{ij}$:

$$\tau_{ij} - \frac{\delta_{ij}}{3}\tau_{kk} = -2\nu_T \overline{S}_{ij}. \tag{6}$$

ν_T is the eddy viscosity and $\overline{S}_{ij} = (\partial \overline{u}_i/\partial x_j + \partial \overline{u}_j/\partial x_i)/2$. Smagorinsky (1963) expressed the eddy-viscosity as

$$\nu_T = C_s^2 \Delta^2 |\overline{S}|, \tag{7}$$

where $|\overline{S}| = (2\overline{S}_{ij}\overline{S}_{ij})^{1/2}$, C_s is the Smagorinsky coefficient and Δ is a length-scale associated with the filter. The Smagorinsky coefficient has to be tuned to a specific flow. In addition damping functions are used to improve performance near walls. In the dynamic model by Germano *et al.* (1991), the eddy viscosity is evaluated without any adjustable constants, and the correct near-wall behavior is captured without any *ad hoc* assumptions. The dynamic approach involves filtering of the flow-field using a filter which is wider than the grid cells. In the mixed Dynamic model by Vreman *et al.* (1994) a similarity model is used together with the Smagorinsky model to express the SGS stresses. Many aspects of SGS models used in LES are discussed in the recent review by Meneveau & Katz (2000). Other reviews are given by Rogallo & Moin (1984) and Lesieur & Métais (1996).

The major constraint on direct and large eddy simulations of turbulent flow is limitations on computer resources. In a turbulent flow, the ratio of the largest to the smallest scales is of order $Re^{3/4}$ (see e.g. Tennekes & Lumley, 1972). In a DNS, where all essential length scales have to be resolved by the computational grid, the necessary number of points in the three-dimensional grid is therefore of order $Re^{9/4}$. In a simulation the number of time-steps needed is of order $Re^{4/3}$. The cost of a DNS of the Navier-Stokes equations is therefore at least proportional to Re^3.

Even for low and moderate Reynolds numbers it is not possible to perform a DNS of an entire experimental configuration. In simulations, both DNSs and LESs, only a part of the flow is therefore considered. Boundary conditions at

open boundaries in the flow must therefore be specified. In flows having statistical homogeneous directions, periodic boundary conditions are imposed. For complex flow and spatially developing flows this is not possible and inflow and outflow conditions are required. The fully developed turbulent boundary layer is slowly evolving in the streamwise direction. Spalart (1988) used a coordinate transformation to be able to do a DNS of this flow. Recently, Lund *et al.* (1998) presented a simplified version of this approach. Slowly spatial developing flows were treated without involving any coordinate transformation. More complex flows, such as the flow over a backwards-facing step (Le *et al.*, 1997), have been simulated by essentially allowing random disturbances to develop into realistic turbulence in a rather long region before the region of interest. Another way of generating the inflow conditions has been to feed the inflow boundary with instantaneous velocity components obtained from a separate simulation (see e.g. Na & Moin, 1998; Aksevoll & Moin, 1996). The exit boundary condition in these simulations are based on convective conditions assuming that the turbulence structures smoothly leaves the computational domain. Still, the problem of generating realistic boundary conditions is a major constraint to simulating complex flows.

In order to simulate the flow between a rotating and a stationary disk without an outer shroud, flow conditions at an open boundary in the flow have to be specified. In this work, a first suggestion of how to treat the boundary conditions and how to construct the computational domain, was to use a rectangular grid and a computer code using Cartesian coordinates to solve the governing equations. By centering the computational domain at the axis of the rotating disk, periodicity could be imposed between grid-points being located directly opposite of the axis of rotation. This is indicated by the points P_1 and P_2 in figure 3. An advantage of a Cartesian over a cylindrical grid is that the singularity at $r = 0$ and the decreasing size of the grid cells near $r = 0$ is avoided. The computer code ECCLES (see next section) was modified to incorporate this periodicity.

Since we are interested in the turbulent part of the flow, this computational domain includes the laminar region near the axis of rotation as well as the transitional and turbulent regions. As a result, an estimate of the necessary number of grid-points shows that a simulation is not possible with available computer resources. In the turbulent regime for small-clearance flow, Daily & Nece (1960) found the empirical correlation for the moment coefficient:

$$C_m \equiv \frac{2\pi \int_0^R r^2 \tau_\theta dr}{1/2 \rho \omega^2 R^5} = 0.04\, G_R^{-1/6}\, Re_R^{-1/4}. \tag{8}$$

Here τ_θ is the tangential component of the shear stress at the rotor. From the definition of C_m it is seen that

$$\frac{\partial C_m}{\partial R} = \frac{4\pi\, \tau_\theta}{\rho \omega^2 R^3} - \frac{5}{R} C_m \tag{9}$$

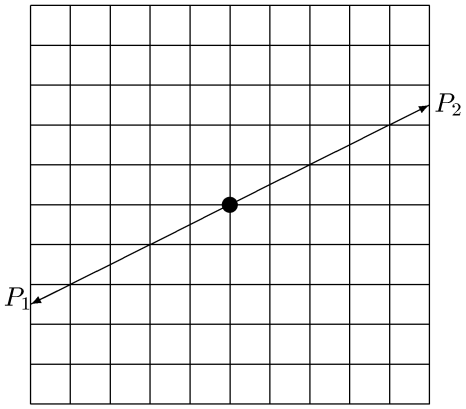

Figure 3: Sketch of the computational domain for the flow between disks using Cartesian coordinates. The axis of rotation is indicated by the filled circle. Periodicity is assumed between r and $-r$.

and from the correlation in equation (8)

$$\frac{\partial C_m}{\partial R} = 0.04 \left(\frac{\partial G_R^{-1/6}}{\partial R} Re_R^{-1/4} + G_R^{-1/6} \frac{\partial Re_R^{-1/4}}{\partial R} \right) = -0.04/3 \; G_R^{-1/6} \; Re_R^{-1/4}. \tag{10}$$

Cooper & Reshotko (1975) assumed that the local radius r may be substituted for R in the empirical relation in equation (8). Using this assumption, equations (8) through (10) may be combined to give the local shear stress coefficient

$$\frac{\tau_\theta(r)}{\rho\omega^2 r^2} = 0.0149 \, G_r^{-1/6} \; Re_r^{-1/4}. \tag{11}$$

$G_r = s/r$ is the local gap ratio. The local Reynolds number based on the tangential component of the shear stress and the gap spacing may now be estimated:

$$Re_\tau = \frac{u_\tau s}{\nu} = \frac{\tau_\theta(r)}{\rho\omega^2 r^2} \frac{sr\omega}{\nu} = 0.122 \, G_r^{11/12} \; Re_r^{7/8}. \tag{12}$$

Now, suppose we wanted to use the Cartesian grid sketched in figure 3 to simulate a flow which has completed the transition to turbulence at a smaller radius than L where $2L$ is the length of the sides of the computational domain. Assuming that the rotational Reynolds number Re_r at $r = L$ is $4 \cdot 10^5$ and the gap ratio $s/L = 0.02$, the corresponding Re_τ at $r = L$ from equation (12) is 270. In wall units the extension of the computational domain then becomes $(2L)^+ = 2Re_\tau L/s = 2.7 \cdot 10^4$. If 100 grid points are used in the axial direction,

and a grid spacing of 10 wall units is allowed in the two directions parallel to the disks, the total number of grid points is $2700 \times 2700 \times 100 \approx 7 \cdot 10^8$. This number is approximately 2 orders of magnitude larger than what is feasible with the memory available on CRAY J90, which is the computer used in this thesis.

Therefore the Cartesian approach had to be abandoned. However the boundary treatment outlined above could be used as an alternative to conventional periodic boundary conditions used in channel flow and plane Couette flow simulations. As described in section 5, several simulations of turbulent plane Couette flow have revealed a pattern of large scale structures which is not observed experimentally. In order to study the influence of the boundary conditions on these structures, the simulations in papers VI and VII are based on different versions of the boundary treatment illustrated in figure 3.

To achieve the resolution requirements in DNS of turbulent flows, a method originally developed by Wu & Squires (2000) was used in the disk simulations in the present thesis. Wu & Squires (2000) studied the turbulent flow in the boundary layer over one rotating disk. Their main idea was to use cylindrical coordinates and locate the computational domain in the turbulent part of the flow. Here, the computational domain consists of an angular section limited by two radial planes r_1 and r_2, see figure 2 in paper I. In the axial direction the domain is limited by the two disks. At the disks no-slip conditions are imposed and periodic conditions are used in the tangential direction. Between the radial planes r_1 and r_2 quasi-periodic conditions are specified. This approach is carefully explained in paper I.

This approach allowed us to study the flow at two different gap distances, one small and one large. For each gap, the computational domain is placed at different radial positions, thus simulating the flow at different rotational Reynolds numbers. Table 4 shows the computational domain parameters for the different simulations.

5 Plane Couette flow

Two papers in this thesis describe simulations of the turbulent plane Couette flow. The plane Couette flow, which is one of the canonical flow configurations, is the flow between two parallel, infinite planes that move relative to each other with a constant velocity. Figure 4 shows a sketch of the flow. The plane Couette flow is the simplest shear-driven flow. The profile of the tangential velocity component in rotor-stator flows having small gap ratios resembles the profile in turbulent plane Couette flow. In fact, as discussed in paper III, in the limit $s/r \to 0$ the rotor-stator flow will locally approach the plane Couette flow.

The main motivation for studying the plane Couette flow here, is that the non-conventional periodic boundary conditions described above, and a accompanying multigrid Poisson solver allowed us to investigate the influence of the streamwise boundary conditions on very-large-scale structures found in numerically generated Couette flow. In several direct numerical simulations of the Couette flow one has observed a periodic array of large-scale vortices, see Lee &

Re_r	G_r	Re_τ	N_θ	N_r	N_z	L_θ	L_r
$4 \cdot 10^5$	0.02	266-214	192	192	128	7	3.5
DNS			$(r_m \Delta\theta)^+$	Δr^+	Δz^+	L_θ^+	L_r^+
			10	5	0.42-4	1862	931
Re_r	G_r	Re_τ	N_θ	N_r	N_z	L_θ	L_r
$4 \cdot 10^5$	0.02	268-214	96	48	48	14	3.5
LES			$(r_m \Delta\theta)^+$	Δr^+	Δz^+	L_θ^+	L_r^+
			39	20	0.55-9	3754	938
Re_r	G_r	Re_τ	N_θ	N_r	N_z	L_θ	L_r
$1 \cdot 10^6$	0.0126	381-349	96	64	64	10	3.5
LES			$(r_m \Delta\theta)^+$	Δr^+	Δz^+	L_θ^+	L_r^+
			40	21	0.54-10	3810	1334
Re_r	G_r	Re_τ	N_θ	N_r	N_z	L_θ	L_r
$1.6 \cdot 10^6$	0.01	460-426	96	64	64	8	3
LES			$(r_m \Delta\theta)^+$	Δr^+	Δz^+	L_θ^+	L_r^+
			38	22	0.58-12	3680	1380
Re_r	G_r	Re_τ	N_θ	N_r	N_z	L_θ	L_r
$6.4 \cdot 10^5$	0.1	2050-1534	128	128	128	3	1.5
LES			$(r_m \Delta\theta)^+$	Δr^+	Δz^+	L_θ^+	L_r^+
			48	24	0.5-25	6150	3075
Re_r	G_r	Re_τ	N_θ	N_r	N_z	L_θ	L_r
$1.6 \cdot 10^6$	0.0632	2856-2564	128	128	192	2	1
LES			$(r_m \Delta\theta)^+$	Δr^+	Δz^+	L_θ^+	L_r^+
			45	22	0.58-26	5712	2856

Table 1: Computational domain parameters for the disk simulations reported in this thesis. In the definitions of Reynolds numbers and gap ratios the radial position in the middle of the computational domains is used, i.e. $r_m = (r_1 + r_2)/2$. The Reynolds number Re_τ is based on the tangential friction velocity, i.e. $Re_\tau = u_{\theta\tau} s/\nu$ where $u_{\theta\tau} = (\nu \partial U_\theta/\partial z)^{1/2}$. The two numbers of Re_τ correspond to the friction at the rotating disk (highest values) and at the stationary disk (lowest values). The friction velocity at the rotating disk is used when expressing lengths in wall-units.

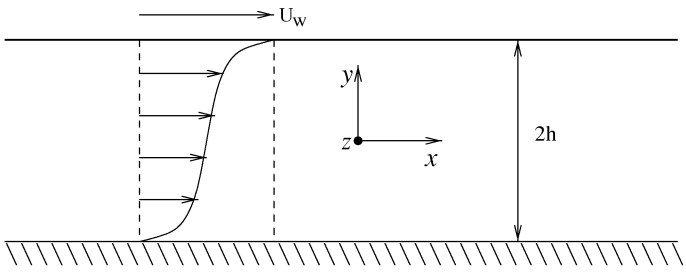

Figure 4: Sketch of the turbulent plane Couette flow.

Kim (1991); Kristoffersen *et al.* (1993); Bech *et al.* (1995); Bech & Andersson (1994) and Papavassiliou & Hanratty (1997). Bech & Andersson (1994) observed that the size of the computational domain influenced the development of the large-scale vortices. Especially when the spanwise length of the computational domain allowed pairs of counter-rotating vortices to be contained in the domain, strong vortices have been observed in simulations. In contrast, persistent pairs of counter-rotating vortices have not been observed experimentally in the plane Couette flow.

Ideally, when periodic boundary conditions are used in direct numerical simulations, two-point correlations of the flow variables should be zero at separations corresponding to half the length of the computational boxes. In simulations of the plane Couette flow, this requirement has been very difficult to fulfill due to the presence of the large-scale structures. Even in the extremely large computational domain used by Komminaho *et al.* (1996), the correlations did not drop to zero. In paper VI it is hypothesized that persistent large-scale vortices are a numerical artifact and that use of periodic boundary conditions may amplify their formation. To test this hypothesis simulations are performed where ordinary periodicity in the streamwise direction is replaced by two sets of boundary conditions using an alternative non-conventional periodicity. Since the study of the plane Couette flow is not the main aim of this project, a modest computer cost is required. Therefore the number of grid-points is low. The size of the computational domain is correspondingly rather small and equals the one used in the simulation in Kristoffersen *et al.* (1993).

6 Numerical approach

The computer codes used in this thesis are modified versions of the research code ECCLES (Explicit Channel Code for Large Eddy Simulation) developed by Gavrilakis *et al.* (1986). ECCLES uses second-order finite-difference approximations in space. The velocity field is advanced in time using an explicit Adams-Bashforth scheme together with the projection method to obtain continuity of the velocity field. The specific steps for the solution of the time-dependent incompressible Navier-Stokes equations are:

1. At time-step n a tentative velocity field u_i^* is calculated from

$$\frac{u_i^* - u_i^n}{\Delta t} = \frac{3}{2} H_i^n - \frac{1}{2}\left(H_i^{n-1} - \frac{\partial p^{n-1}}{\partial x_i} \right). \tag{13}$$

Here, H_i^n is defined as the sum of the nonlinear, subgrid and viscous terms at time step n.

2. The pressure p^n is found by solving the Poisson-equation

$$\frac{\partial^2 p^n}{\partial x_j \partial x_j} = \frac{2}{3\Delta t} \frac{\partial u_j^*}{\partial x_j} \tag{14}$$

3. Finally, the velocity field for the next time-step $n+1$ is found using a corrected u_i^*: correction

$$u_i^{n+1} = u_i^* - \frac{3}{2}\Delta t \frac{\partial p^n}{\partial x_i} \tag{15}$$

ECCLES is a code designed for simulating plane channel flows, and Cartesian coordinates are therefore used. To facilitate simulations of the rotor-stator flow, a code in cylindrical coordinates is needed. The computational domain used in the present rotor-stator simulations does not include the origin $r = 0$. ECCLES could therefore be transformed to cylindrical coordinates in a straight forward manner. Finite difference schemes intending to include the region at $r = 0$ need a special treatment to account for the singularity there, see e.g. Verzicco & Orlandi (1996).

Since the scheme outlined above is explicit, only the Poisson equation is solved. ECCLES was developed to simulate flow between parallel plates and homogeneous streamwise and spanwise directions allowed periodic boundary conditions to be used. The Poisson equation may then be solved directly using fast Fourier transformations in the homogeneous directions and a tridiagonal solver in the wall-normal direction. Neither the non-standard boundary conditions used in simulating the plane Couette flow nor the boundary conditions in the radial direction in the rotor-stator flows, allow Fourier transformations to be used in two directions. Therefore, a new fast Poisson solver is implemented in the code.

6.1 A multigrid Poisson solver

We require that the Poisson solver has to fulfill the following requirements: (i) It must be fast since equation 14 has to be solved on every time-step in a DNS. (ii) Storage requirements must be kept low. (iii) The solver has to be vectorizable. (iv) It must handle a stretched grid in the wall-normal direction and grid cells with a very small wall-normal length compared to the other two directions.

Classical iterative methods like Gauss-Seidel and SOR suffer, especially in three dimensions, from slow convergence rates. To increase the efficiency of iterative schemes used to solve boundary value problems on spatial domains, multigrid methods have been developed during the last decades. In the following only a rough outline of the methods is given. For a more detailed description, the references listed below may be consulted.

The main idea of the multigrid method is to take advantage of the smoothing capability of some of the classical solvers. These solvers damp high frequency oscillations after just a few relaxations. When transferring this smooth approximation to a coarser grid, the approximation will appear more high-frequent. On the coarser grid we continue to iterate to get a new approximation. The coarse grid approximation may then be transfered back to the fine grid and used to adjust the fine-level-solution, thus completing a 2-level multigrid V-cycle. Generally a M-level V-cycle is used where we zoom down to the coarsest possible grid.

Several textbooks and articles describing multigrid methods exist. Important references are books by Hackbush (1985) and Wesseling (1992), as well as the article by Brandt (1977). In the implementation of the multigrid algorithm, the tutorial by Briggs (1987) has been very useful, together with the report by Kristoffersen (1994).

Multigrid algorithms using different smoothers were tested on the Poisson equation

$$\frac{\partial^2 p}{\partial x_j \partial x_j} = \cos\left(\frac{2\pi}{l_x}x\right)\cos\left(\frac{2\pi}{l_y}y\right)\cos\left(\frac{2\pi}{l_z}z\right), \tag{16}$$

where the size of the computational domain was $l_x \times l_y \times l_z$. Periodic boundary conditions were used in the x and y directions, while the normal derivative is zero at the z-facing boundaries. The analytical solutions of this problem is

$$p(x,y,z) = -\frac{1}{(\frac{2\pi}{l_x})^2 + (\frac{2\pi}{l_y})^2 + (\frac{2\pi}{l_z})^2}\cos\left(\frac{2\pi}{l_x}x\right)\cos\left(\frac{2\pi}{l_y}y\right)\cos\left(\frac{2\pi}{l_z}z\right). \tag{17}$$

Repeated V-cycles were used in the multigrid algorithm. To compare different solution methods a *work unit* (WU) is defined as the cost of performing one iteration on the finest grid. In the two test-cases presented here, two smoothers have been tested in the multigrid algorithm. These are the classical Gauss-Seidel iteration scheme and the so-called Line-Zebra Gauss-Seidel scheme. The Gauss-Seidel scheme is organized in a chess-board pattern. This way points within the grid are decoupled allowing for vectorization and parallelization. An ordinary Line Gauss-Seidel iteration scheme consists in solving the discretized scheme along coordinate lines in the domain. For the Poisson equation using second-order differences, a three-diagonal matrix has to be inverted for every line. A complete iteration consists in solving along every line in a given direction. A Line-Zebra Gauss-Seidel scheme solve for every second line in a chess-board pattern in order to be able to vectorize the scheme.

In the development of the multigrid solver, various tests were performed to study the performance of different schemes and smoothers. The two test-cases reported here are included in this introduction in order to give an impression of the performance of the multigrid scheme. The tests shown are for a rectangular grid. When implemented in cylindrical coordinates the behavior of the different smoothers did not change significantly. For comparisons with schemes which are not using the multigrid algorithm, the performance of ordinary Gauss-Seidel and SOR iterations are shown. The over-relaxation parameter in the SOR iterations is tuned to give the fastest convergence in the different cases.

Test-case 1

The domain size and number of grid cells are $l_x \times l_y \times l_z = 1 \times 1 \times 1$ and $N_x \times N_y \times N_z = 64 \times 64 \times 64$. The grid-spacing is equal in all directions. The initial field consist of random numbers between $\pm 1/((\frac{2\pi}{l_x})^2 + (\frac{2\pi}{l_y})^2 + (\frac{2\pi}{l_z})^2)$. The convergence history for the errors is given in figure 5. The errors are based on solution of the discretized equations. Multigrid solutions using the Gauss-Seidel

and the Line-Zebra Gauss-Seidel smoothers are labeled "GS_{MG}" and "LZ_{MG}", respectively. This figure clearly shows the superiority of multigrid solvers as compared to ordinary single-grid solvers.

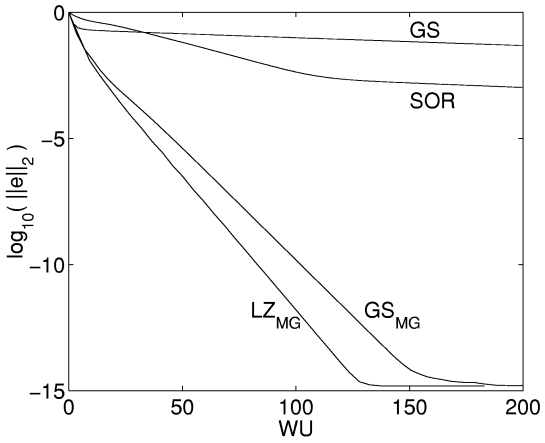

Figure 5: Convergence histories of the errors as function of work unit (WU) for case 1.

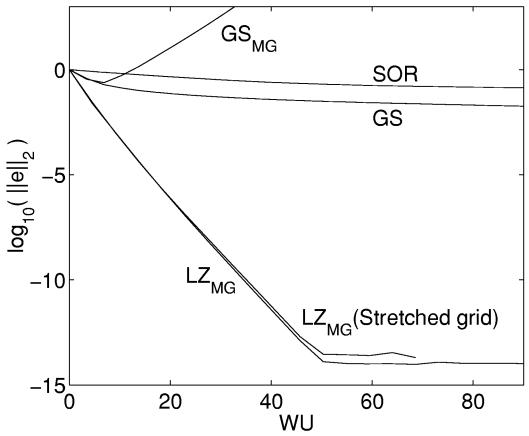

Figure 6: Convergence histories of the errors as function of work unit (WU) for case 2.

Test-case 2

In this case the domain size is $l_x \times l_y \times l_z = 4\pi \times 2\pi \times 1$. Otherwise case 2 is equal to case 1. The domain size is now more similar to those used in DNS of channel flows. The convergence history is given in figure 6. For this domain size

the Gauss-Seidel smoother completely fails in the multigrid algorithm due to the high aspect-ratio of the grid cells. Therefore the ordinary Gauss-Seidel iterations can not be used as smoother here. The Line-Zebra smoother is further tested on a grid which is strongly stretched in the z-direction. This stretching is similar to the grid-refinement in simulations of wall-bounded flows. Figure 6 shows that this stretching does not influence the convergence history for the Line-Zebra Gauss-Seidel smoother. For this reason this smoother is implemented in the multigrid solver.

Summary of papers

Five of the following seven papers are related to the flow between a rotating and a stationary disk (papers I-V). Paper VI and VII relates to the turbulent plane Couette flow.

Paper I **Turbulent flow between a rotating and a stationary disk**
A direct numerical simulation is performed of the turbulent flow in the narrow gap in a simplified rotor-stator configuration consisting of "infinite" disks. The effect of mean-flow three-dimensionality leads to a misalignment between the Reynolds shear stress vector and the mean velocity gradient vector. In addition there is a reduction in production of Reynolds shear stress. Conditional averages of the near-wall coherent vortices show that vortices of different sign of rotation generate different amount of turbulence shear stress. This is also an effect of the three-dimensionality of the mean flow.
J. Fluid Mech., 2001, **426**, 297-326

Paper II **Near-wall structures in turbulent rotor-stator flow**
Ensemble averages, probability-density functions and a quadrant analysis of the velocity field in the near-wall regions of the flow presented in paper I, show that the strength of sweeps associated with the coherent vortical structures in the near-wall region was reduced.
In *Advances in Turbulence VIII*, 2000, CIMNE, Barcelona, 675-678.

Paper III **Turbulence statistics in an open rotor-stator configuration**
Turbulence statistics, including complete budget data for the six independent components of the Reynolds stress tensor, have been compiled from the direct numerical simulation in paper I. The direct impact of the rotation term in the transport equations is low, but the effect of rotation is still evident in the development of the Reynolds stress tensor.
Submitted for publication

Paper IV **Large eddy simulations of the turbulent flow between a rotating and a stationary disk**

A dynamic and a mixed dynamic subgrid-scale model are used in large eddy simulations. The simulations are compared to the simulation presented in paper I. The mixed dynamic model gave better overall predictions than the dynamic model.

To appear in proceedings from the *Second International Symposium on Turbulence and Shear Flow Phenomena*, 2001, Stockholm.

Paper V **Effects of Reynolds number and gap ratio on open rotor-stator flow**

Simulations are performed of a narrow- and a large-gap rotor-stator flow. The flow is studied at different radial positions of both gap-widths. As the radial position increases, the degree of mean-flow three-dimensionality decreases. This is reflected in the turbulence statistics and in modifications of near-wall coherent structures caused by the three-dimensionality.

To be submitted for publication in 2001

Paper VI **Roll Cells in Turbulent Plane Couette Flow: Reality or Artifact?**

A special set of boundary conditions is used in a direct numerical simulation of the turbulent plane Couette flow. The aim is to break the inflow–outflow coupling associated with periodic boundary conditions and to study the effect of the boundary conditions on the very-large-scale structures observed in numerically generated Couette flows. To facilitate the simulation, a multigrid Poisson solver is developed.

In *16th International Conference in Numerical Methods in Fluid Dynamics*, 1998, Archachon, ed. C.H. Bruneau, pp. 117-122, Springer

Paper VII **Influence of boundary conditions on the large-scale structures in turbulent plane Couette flow**

In addition to the boundary conditions used in Paper VI, a similar non-conventional boundary treatment is applied in simulations of the Couette flow. The effect of the boundary conditions is to shorten the streamwise length-scale of the structures as well as to reduce the tendency for roll cells to develop. However, firm conclusions regarding the existence of the vortices could not be drawn, mainly due to the small extension of the computational domain used.

In *First International Symposium on Turbulence and Shear Flow Phenomena*, 1999, Santa Barbara, California, eds. S. Banerjee and J.K. Eaton, pp. 15-20, Begell House

Bibliography

Aksevoll, K. & Moin, P. 1996 Large-eddy simulation of turbulent confined coannular jets. *J. Fluid Mech.* **315**, 387–411.

Batchelor, G. K. 1951 Note on a class of solutions of the Navier-Stokes equations representing steady rotationally-symmetric flow. *Quart. J. Mech. Appl. Math.* **4**, 29–41.

Bech, K. H. & Andersson, H. I. 1994 Very-large-scale structures in DNS. *Direct and Large-Eddy Simulation I,* Kluwer pp. 13–24.

Bech, K. H., Tillmark, N., Alfredsson, P. H. & Andersson, H. I. 1995 An investigation of turbulent plane Couette flow at low Reynolds numbers. *J. Fluid Mech.* **286**, 291–325.

Bodewadt, U. T. 1940 Die drehstronung uber festem grunde. *Z. Angew. Math. Mech* **27**, 241–253.

Bradshaw, P. & Pontikos, N. S. 1985 Measurements in the turbulent boundary layer on an 'infinite' swept wing. *J. Fluid Mech.* **159**, 105–130.

Brandt, A. 1977 Multi-level adaptive solutions to boundary-value problems. *Math. Comp.* **31**, 333–390.

Briggs, W. I. 1987 *A multigrid tutorial*. Philadelphia: SIAM.

Cheah, S. C., Iacovides, H., Jackson, D. C., Ji, H. & Launder, B. E. 1994 Experimental investigation of enclosed rotor-stator disk flows. *Exp. Thermal Fluid Sci.* **9**, 445–455.

Coleman, G. N., Ferziger, J. H. & Spalart, P. R. 1990 A numerical study of the turbulent Ekman layer. *J. Fluid Mech.* **213**, 313–348.

Coleman, G. N., Kim, J. & Moser, R. D. 1995 A numerical study of turbulent supersonic isothermal-wall channel flow. *J. Fluid Mech.* **305**, 159–183.

Coleman, G. N., Kim, J. & Spalart, P. R. 2000 A numerical study of strained three-dimensional wall-bounded turbulence. *J. Fluid Mech.* **416**, 75–116.

Cooper, P. & Reshotko, E. 1975 Turbulent flow between a rotating disk and a parallel wall. *AIAA J.* **13**, 573–578.

Daily, J. W. & Nece, R. E. 1960 Chamber dimension effects on induced flow and frictional resistance of enclosed rotating disks. *ASME J. Basic Engng* **82**, 217–232.

Elena, L. & Schiestel, R. 1995 Turbulence modeling of confined flow in rotating-disk systems. *AIAA J.* **33**, 812–821.

Gauthier, G., Gondret, P. & Rabaud, M. 1999 Axisymmetric propagating vortices in the flow between a stationary and a rotating disk enclosed by a cylinder. *J. Fluid Mech.* **386**, 105–126.

Gavrilakis, S., Tsai, H. M., Voke, P. R. & Leslie, D. C. 1986 Large-eddy simulation of low Reynolds number channel flow by spectral and finite difference methods. *Notes on Numerical Fluid Mechanics,* Vieweg **15**, 105–118.

Germano, M., Piomelli, U., Moin, P. & Cabot, W. H. 1991 A dynamic subgrid-scale eddy viscosity model. *Phys. Fluids* **A 3**, 1760–1765.

Hackbush, W. 1985 *Multi-grid methods and applications*. Berlin: Springer.

Holodniok, M., Kubicek, M. & Hlavacek, V. 1977 Computation of the flow between two rotating coaxial disks. *J. Fluid Mech.* **81**, 689–699.

Holodniok, M., Kubicek, M. & Hlavacek, V. 1981 Computation of the flow between two rotating coaxial disks: multiplicity of steady-state solutions. *J. Fluid Mech.* **108**, 227–240.

Itoh, M. 1995 Experiments on the turbulent flow in the narrow clearance between a rotating and a stationary disk. In: *Turbulent Flows, ASME-FED* **208**, 27–32.

Itoh, M., Yamada, Y., Imao, S. & Gonda, M. 1992 Experiments on turbulent flow due to an enclosed rotating disk. *Exp. Thermal Fluid. Sci.* **5**, 359–368.

von Karman, T. 1921 Uber laminare und turbulente reibung. *Z. Angew. Math. Mech.* **1**, 233–252.

Keller, H. & Szeto, R. 1980 Calculation of flows between rotating disks. In *Computing Methods in Applied Sciences and Engineering* (ed. L. J. Glowinsky, R.), pp. 51–61. Amsterdam: North-Holland.

Kilic, M., Gan, X. & Owen, J. 1996 Turbulent flow between two disks contrarotating at different speeds. *Trans. ASME* **118**, 408–413.

Kim, J., Moin, P. & Moser, R. 1987 Turbulence statistics in fully developed channel flow at low Reynolds number. *J. Fluid Mech.* **177**, 133–166.

Komminaho, J., Lundbladh, A. & Johansson, A. V. 1996 Very large structures in plane turbulent Couette flow. *J. Fluid Mech.* **320**, 259–285.

Kristoffersen, R. 1994 *A Navier-Stokes solver using the multigrid method*. Trondheim: MTF-Report 1994:106.

Kristoffersen, R. & Andersson, H. I. 1993 Direct simulation of low-Reynold-number turbulent flow in a rotating channel. *J. Fluid Mech.* **256**, 163–197.

Kristoffersen, R., Bech, K. H. & Andersson, H. I. 1993 Numerical study of turbulent plane Couette flow at low Reynolds number. *Appl. Sci. Res.* **51**, 337–343.

Lance, G. N. & Rogers, M. H. 1962 The axially symmetric flow of a viscous fluid between two infinite rotating disks. *Proc. Roy. Soc. A* **266**, 109.

Launder, B. & Sharma, B. 1974 Application of the energy-dissipation model of turbulence to the calculation of the low near a spinning disk. *Letters in heat and mass transfer* **1**, 131–138.

Le, A.-T., Coleman, G. N. & Kim, J. 1999 Near-wall turbulence structures in three-dimensional boundary layers. In *Turbulence and Shear Flow Phenomena - 1* (ed. S. Banerjee & J. K. Eaton), pp. 151–156. Begell House, inc.

Le, H., Moin, P. & Kim, J. 1997 Direct numerical simulation of turbulent flow over a backward facing step. *J. Fluid Mech.* **330**, 349–374.

Lee, M. J. & Kim, J. 1991 The structure of turbulence in a simulated plane Couette flow. *8th Symposium on Turbulent Shear Flows,* Munich pp. 5.3.1–5.3.6.

Lee, S., Lele, S. K. & Moin, P. 1997 Interaction of isotropic turbulence with shock waves. *J. Fluid Mech.* **340**, 225–247.

Lesieur, M. & Métais 1996 New trends in large-eddy simulations of turbulence. *Ann. Rev. Fluid Mech.* **28**, 45–82.

Littell, H. S. & Eaton, J. K. 1994 Turbulence characteristics of the boundary layer on a rotating disk. *J. Fluid Mech.* **266**, 175–207.

Lund, T. S., Wu, X. & Squires, K. D. 1998 Generation of turbulent inflow data for spatially-developing boundary layer simulations. *J. Comp. Phys.* **140**, 233–258.

Mellor, G., Chapple, P. & Stokes, V. 1968 On the flow between a rotating and a stationary disk. *J. Fluid Mech.* **31**, 95–112.

Meneveau, C. & Katz, J. 2000 Scale-invariance and turbulence models for large-eddy simulation. *Ann. Rev. Fluid Mech.* **32**, 1–32.

Moin, P. & Mahesh, K. 1998 Direct numerical simulation: A tool in turbulent research. *Ann. Rev. Fluid Mech.* **30**, 539–578.

Moin, P., Shih, T. H., Driver, D. & Mansour, N. N. 1990 Direct numerical simulation of a three-dimensional turbulent boundary layer. *Phys. Fluids A* **2**, 1846–1853.

Morse, A. 1991 Assessment of laminar-turbulent transition in closed disk geometries. *J. Turbomachinery* **113**, 131–138.

Moser, R. & Moin, P. 1987 The effects of curvature in wall-bounded turbulent flows. *J. Fluid Mech.* **175**, 479–510.

Na, Y. & Moin, P. 1998 Direct numerical simulation of a separated turbulent boundary layer. *J. Fluid Mech.* **370**, 175–201.

Nguyen, N., Ribault, J. & Florent, P. 1975 Multiple solutions for flow between coaxial disks. *J. Fluid Mech.* **68**, 369–388.

Orszag, S. & Patterson, G. 1972 Numerical simulation of three-dimensional homogeneous isotropic turbulence. *Phys. Rev. Lett.* **28**, 79–79.

Owen, J. M. & Rogers, R. H. 1989 *Flow and Heat Transfer in Rotating-Disc Systems, Volume 1 – Rotor-Stator Systems*. Resarch Studies Press, Taunton (John Wiley).

Papavassiliou, D. V. & Hanratty, T. J. 1997 Interpretation of large-scale structures observed in a turbulent plane Couette flow. *Int. J. Heat Fluid Flow* **18**, 55–69.

Pearson, C. 1965 Numerical solutions for the time-dependent viscous flow between two rotating coaxial disks. *J. Fluid Mech.* **21**, 623–633.

Randriamampianina, A., Elena, L., Fontaine, J. & Schistel, R. 1997 Numerical prediction of laminar, transitional and turbulent flows in shrouded rotor-stator systems. *Phys. Fluids* **9**, 1696–1713.

Roberts, S. & Shipman, J. 1976 Computation of the flow between a rotating and a stationary disk. *J. Fluid Mech.* **73**, 53–63.

Rogallo, R. S. & Moin, P. 1984 Numerical simulation of turbulent flows. *Ann. Rev. Fluid Mech.* **16**, 99–137.

Schouveiler, L. 1998 Sur les instabilites des ecoulements entre un disque fixe et un disque en rotation. *PhD thesis, Universite Aix-Marseille II* .

Schouveiler, L., Le Gal, P., Chauve, M. P. & Takeda, Y. 1999 Spiral and circular waves in the flow between a rotating and a stationary disk. *Exp. Fluids* **26**, 179–187.

Smagorinsky, J. 1963 General circulation experiments with the primitive equations. i. the basic experiment. *Mon. Weather Rev.* **91**, 99–164.

Spalart, P. R. 1988 Direct simulation of a turbulent boundary layer up to $Re_\theta = 1410$. *J. Fluid Mech.* **187**, 61–98.

Spalart, P. R. 1989 Theoretical and numerical study of a three-dimensional turbulent boundary layer. *J. Fluid Mech.* **205**, 319–340.

Stewartson, K. 1953 On the flow between two rotating coaxial disks. *Proc. Camb. Phil. Soc.* **49**, 333–341.

Szeto, R. 1978 The flow between rotating coaxial disks. *PhD thesis, Calif. Inst. Technol., Pasadena* .

Tennekes, H. & Lumley, J. L. 1972 *A First Course in Turbulence.*. The MIT Press, Cambridge, Mass.

Verzicco, R. & Orlandi, P. 1996 A finite-difference scheme for three-dimensional incompressible flows in cyllindrical coordinates. *J. Comp. Phys.* **123**, 402–414.

Vreman, B., Geurts, B. & Kuerten, H. 1994 On the formulation of the dynamic mixed subgrid-scale model. *Phys. Fluids* **12**, 4057–4059.

Wesseling, P. 1992 *An introduction to multigrid methods*. John Wiley & Sons.

Wu, X. & Squires, K. D. 2000 Prediction and investigation of the turbulent flow over a rotating disk. *J. Fluid Mech.* **418**, 231–264.

Zandbergen, P. J. & Dijkstra, D. 1987 Von Karman swirling flows. *Ann. Rev. Fluid Mech.* **19**, 465–491.

The following papers are not included in the PDF-file :

Paper I: Lygren, M & Andersson H. I. 2000 Turbulent flow between a rotating and a stationary disk. *J. Fluid Mech*. **426**, 297-326.

Paper II: Lygren, M. & Andersson H. I. 2000 Near-wall structures in turbulent rotor-stator flow. In *Advances in turbulence VIII, Proceedings of the Eighth European Turbulence Conference* (ed. C. Dopazo et al.), CIMNE, Barcelona.

Paper III: Lygren, M. & Andersson H. I. 2002 Turbulence statistics in an open-stator configuration. *Physics of Fluids*. **14**, 3, 1137-1145.

Paper IV: Lygren, M. & Andersson H. I. 2001 Large eddy simulations of the turbulent flow between a rotating and a stationary disk. In *Turbulence and Shear Flow Phenomena 2, Volume II*, Second International Symposium on Turbulence and Shear Flow Phenomena, Stockholm.

Paper V: Lygren, M. 2001. Effects of Reynolds number and gap ratio on open rotor-stator flow

Paper VI: Andersson, H. I., Lygren M. & Kristoffersen, R. 1998 Roll Cells in Turbulent Plane Couette Flow: Reality or Artifact? In *16th International Conference in Numerical Methods in Fluid Dynamics* (ed. CH. Bruneau), pp. 117-122. Springer.

Paper VII: Lygren, M. & Andersson, H. I. 1999 Influence of boundary conditions on the large-scale structures in turbulent plane couette flow. In *1st International symposium on turbulence and shear flow phenomena* (eds. S. Banerjee & J. K. Eaton), pp. 15-20, Begell House.